Ceramics International xx (xxxx) xxxx–xxxx

Contents lists available at ScienceDirect

Ceramics International

journal homepage: www.elsevier.com/locate/ceramint

Synthesis and characterization of Ca doped $LaMnO_3$ as potential anode material for solid oxide electrolysis cells

Arup Mahata, Pradyot Datta*, Rajendra N. Basu*

Fuel Cell and Battery Division, CSIR-Central Glass And Ceramic Research Institute, Kolkata 700032, India

ARTICLE INFO

Keywords:
Oxide materials
Chemical synthesis
Thermal expansion
Electrical conductivity

ABSTRACT

There is a need for investigating new electrode materials for solid oxide electrolysis cells (SOEC) as conventional electrodes for solid oxide fuel cells (SOFC) have some limitations when they are used in SOEC mode. Sr substituted $LaMnO_3$ (LSM) is reported to have some demerits when it is used as an anode material in SOEC. With the intention of finding new anode material for SOEC, a series of materials, where Sr of LSM was either partially or fully substituted by Ca, were synthesized via combustion synthesis method. The synthesized material was found to be phase pure with orthorhombic symmetry. Thermal expansion coefficients (TEC) of all the samples were found to be in the range of $11–12\times10^{-6}\ K^{-1}$. Electrical conductivity was found to increase with increasing Ca-content for the samples where Sr was fully replaced by Ca (LCM) but the same was found to decrease with increasing Ca-content for the partially Sr substituted samples (LSCM). The materials with either partial or total substitution of Sr by Ca were used as an anode material of a coupon cell and tested in SOEC mode. These anode materials were found to be better than LSM in terms of hydrogen production. Also, LCM and YSZ did not react with each other even after a prolonged annealing of 100 h at 1000 °C.

1. Introduction

The growing demand for energy along with depleting fossil fuel resources makes it a necessity to find alternative energy sources which are clean and sustainable. Hydrogen has been considered as one such alternative for next generation energy carrier as it is clean, renewable and portable [1,2]. Among many techniques, production of hydrogen through solid oxide electrolysis cells (SOECs) is a promising one as it offers the potential to be carbon-free when combined with an electricity source such as nuclear power station, or renewable energies such as solar energy and wind power [3]. A SOEC consists of mainly three components: an anode, an electrolyte and a cathode [4]. To be sustainable at the high temperature electrolysis conditions and to get good performance from SOEC, these components must fulfill some basic requirements like chemical compatibility with other components, thermal expansion compatibility, adequate conductivity, porosity, catalytic activity etc. Thus, it is a challenge to explore new materials which can be tailor-made for SOEC.

8 mol% yttrium doped zirconia (YSZ), Ni-YSZ cermet and strontium doped lanthanum manganate (LSM) have been widely used as an electrolyte, cathode and anode material respectively for SOEC operation as these materials meet the primary requirements like matched thermal expansion coefficient ($10.8–11.8\times10^{-6}$/K), high ionic conductivity of electrolyte (~0.01 S/cm) and high electrical conductivity of anode (~200 S/cm) under operating conditions [5–7]. However, LSM cathode is not suitable due to its reaction with YSZ electrolyte at high temperature forming non-conducting lanthanum zirconate phase [8–10]. Moreover, its electrochemical performance decreases at reduced temperature due to the low ionic conductivity of LSM [11,12]. $La_{1-x}Sr_xCoO_3$ (LSC) may also be a promising anode material for SOEC due to its very high mixed conductivity. However, use of LSC as anode material is also limited due to thermal expansion mismatch with the electrolytes [13,14]. Ca is considered to be another effective doping element at the A site of ABO_3 perovskite. Takeda et al. [15] investigated on $La_{1-x}A_xMnO_3$ (A=Ca, Sr) and found excellent oxygen reduction catalytic activity, high electrical conductivity and thermal expansion compatibility with YSZ electrolyte. $La_{0.3}Ca_{0.7}MnO_3$ showed highest activity for oxygen reduction. Jie et al. [16] also worked on $La_{1-x}Ca_xFe_{0.9}Mn_{0.1}O_3$ (x = 0.1, 0.3, 0.5) and found high mixed conductivity (> 100 S/cm) and good thermal matching with common electrolytes.

The main objective of this work is to find novel anode materials with high electrical conductivity, good matching of thermal expansion coefficient with electrolyte (YSZ) and the materials which can prevent the formation of secondary phases at the anode/electrolyte interfaces. It can be seen from $LaMnO_3$-$SrMnO_3$-$CaMnO_3$ ternary phase diagram

* Corresponding authors.
E-mail addresses: pdatta@cgcri.res.in (P. Datta), rnbasu@cgcri.res.in (R.N. Basu).

http://dx.doi.org/10.1016/j.ceramint.2016.09.177
Received 11 August 2016; Received in revised form 17 September 2016; Accepted 25 September 2016
Available online xxxx

[17] that (La, Ca)MnO_3 may be a choice for anode material for SOEC as formation of lanthanum zirconate can be prevented at the electrode/electrolyte interfaces which is one of the main factors in the degradation of electrolysis cell during electrolysis. However, it can be noted that a material should not be designed at the cost of the conductivity. Keeping that in mind, effect of systematically Ca doping on $LaMnO_3$ has been studied. Moreover, as $La_{0.65}Sr_{0.30}MnO_3$ (LSM) is widely reported cathode material in SOFC and has been reported as an unsuitable candidate for SOEC, the partial substitution Sr by Ca is also investigated over this composition for the ready comparison of its performance.

In this paper, two kinds of perovskites $La_{(1-x)}Ca_xMnO_3$ (x = 0.3 to 0.5) and $La_{0.65}Sr_yCa_{(0.3-y)}MnO_3$ (y=0.1 to 0.2) were synthesized by combustion synthesis method. The thermal and electrical properties of the samples were thoroughly characterized and the newly synthesized materials were tested as anode materials in high temperature steam electrolysis.

2. Experimental

2.1. Sample preparation

Ca and Sr doped lanthanum manganites $La_{(1-x)}Ca_xMnO_3$ (LCM) and $La_{0.65}Sr_yCa_{(0.3-y)}MnO_3$ (LSCM) were synthesized by nitrate-alanine combustion synthesis method. Stoichiometric amounts of $La(NO_3)_3{\cdot}6H_2O$ (SISCO Research Laboratories), $Sr(NO_3)_2$ (Merck, India), $Ca(NO_3)_2{\cdot}4H_2O$ (Merck, India), $Mn(CH_3COO)_2{\cdot}4H_2O$ (Merck, India) were dissolved in de-ionized water together with $C_3H_7NO_2$ (SISCO Research laboratories) at nitrate/fuel ratio of 1:1 (considering acetate also as a fuel). The solution was heated on a hotplate maintaining a temperature of about 300 °C with continuous stirring by magnetic stirrer. By evaporation, the solution became condensed, and it finally got ignited spontaneously, resulting amorphous ash-like precursor powder. The powder was calcined at 800 °C for 12 h and fine LCM and LSCM powders were obtained after calcination. Table 1 enlists all the compositions prepared for the present investigation. Sample acronyms as used in the text are also given in Table 1.

2.2. Sintering

The calcined powder was mixed with 2 wt% of binder (PVP) and with required amount of methyl ethyl ketone (MEK) solvent in a mortar and pestle. Taking appropriate mass of powder, circular pellets (20 mm diameter and 1.5 mm thickness) and rectangular bar samples ($25\times10\times2$ mm^3) were compacted using a pressure of about 250 MPa. The circular pellets were used for density measurement using Archimedes principle whereas rectangular bars were used for thermal expansion coefficient and electrical conductivity measurements. The samples were sintered at 1300 °C for 3 h in air atmosphere. The heating rates were 2.5 °C/min and 3 °C/min during heating and cooling, respectively. Theoretical densities and relative densities of all compositions were measured by He-Pycnometry (Micromeritics, AccuPycll 1340) and standard Archimedes principle respectively.

2.3. Sample characterizations

Samples were characterized by using various characterization techniques. Viscous gels of the LCM and LSCM samples (collected at the time of gel formation during combustion synthesis) were analyzed by thermo-gravimetric analysis (TGA) and differential thermal analysis (DTA) (STA 409C, Netzsch, Germany) from room temperature to 1000 °C in air at a heating rate of 10 °C/min. Phase purity of all the compositions was determined by analyzing the XRD data from X-ray diffractometer (PANalytical, Philips, Holland) using monochromatic Cu Kα radiation (λ=0.154 mm), tube voltage 40 kV, tube current 30 mA, scanning 2θ range from 10° to 90°. Surface area of all the compositions was measured after calcination at 800 °C using surface area analyzer (Quantachrome, NOVA 4000e). The shrinkage behavior of a green sample was carried out in the dilatometer at the temperature range from room temperature to 1350 °C (NETZSCH, DIL 402C) with a heating rate of 10 °C/min. The thermal expansion coefficients up to 950 °C were measured by the same dilatometer as mentioned above with a constant heating rate of 10 °C/min.

Electrical conductivity of the sintered samples was measured by DC four-probe method in the temperature range from 750 °C to 950 °C in air using a Power source (Agilent, E3631A) and a Multimeter (Agilent, 34401A). Data were collected at every 50 °C interval. For accuracy, each testing temperature was stabilized at least for 10 min before collecting the data. Pt paste, used at the four terminals, was cured at 950 °C for 2 h before the electrical conductivity measurement.

The synthesized anode materials were mixed with YSZ with 50:50 weight ratio and the mixtures were ball milled for 24 h for the use of anode functional layer (AFL). Anode material was also ball milled for 24 h (AL). A thick film paste was made by required organic medium for both AFL and AL. AFL paste was first screen-printed over NiO-YSZ/YSZ-based half cell of diameter 16 mm followed by screen-printing of AL paste. The detail of NiO-YSZ/YSZ half cell fabrication by tape casting has been reported elsewhere [18]. After screen-printing the samples were fired at 975 °C and finally SOEC full cells (coupon cell) were prepared and tested for SOEC application.

One composition each from two types of materials (LCM and LSCM) was tested in SOEC mode. LCM55 is chosen for LCMs and LSCM6512 for LSCMs. Two cells of each composition were tested. Hydrogen production was measured at four different temperatures from 875 °C to 950 °C at 25° interval. Applied voltage was 1.5 V for both the cases. The released gas from cathode outlet was collected and analyzed in Gas Chromatography (Thermo SCIENTIFIC TRACE GC ULTRA). The detailed experimental set up for SOEC testing is given elsewhere [19].

3. Results

3.1. DTA and TGA study

Combination of DTA and TGA was carried out with the intention of finding out the material formation and to select the calcination temperature of the synthesized powder after combustion synthesis. One representative composition of each group of materials was chosen

Table 1
Sample acronyms and various properties of the as prepared samples.

Compositions	Acronyms	Surface area (m^2/g)	Theoretical density (g/cm^3)	Relative density (%)	TEC values ($\times10^{-6}$ K^{-1})	Conductivity at 950 °C (S/cm)	Activation Enthalpy (kJ/mol)
$La_{0.5}Ca_{0.5}MnO_3$	LCM55	11.1	6.44	98.7	11.19	234	10.3
$La_{0.6}Ca_{0.4}MnO_3$	LCM64	7.6	6.41	97.0	11.56	249	9.1
$La_{0.7}Ca_{0.3}MnO_3$	LCM73	5.8	6.01	92.6	12.28	264	6.8
$La_{0.65}Sr_{0.1}Ca_{0.2}MnO_3$	LSCM6512	17.0	6.63	90.9	11.41	204	8.2
$La_{0.65}Sr_{0.15}Ca_{0.15}MnO_3$	LSCM651515	17.2	6.66	90.1	12.54	208	8.3
$La_{0.65}Sr_{0.2}Ca_{0.1}MnO_3$	LSCM6521	18.0	6.81	88.6	12.16	230	9.2

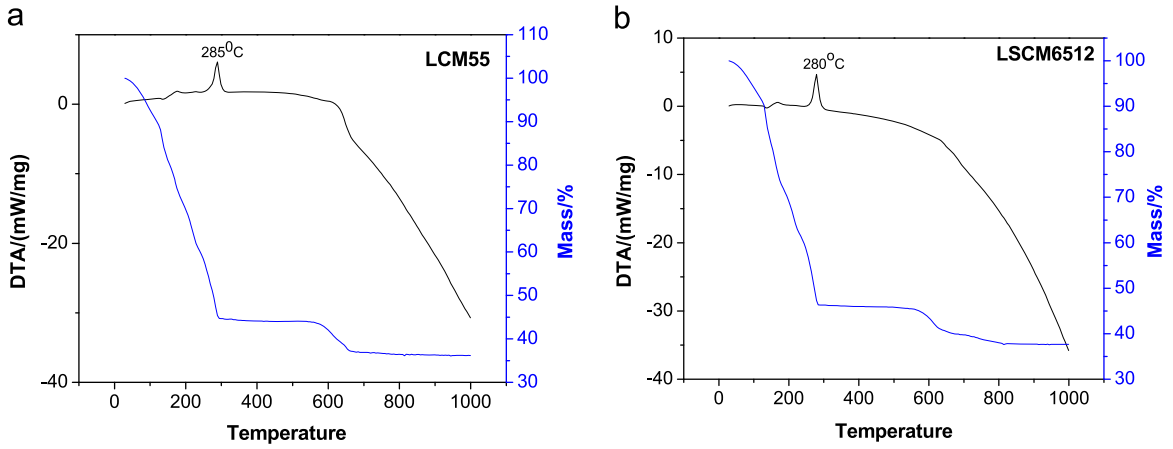

Fig. 1. a and b: TGA and DTA curves of LCM55 and LSCM6512.

for this purpose. Fig. 1a and b shows the TGA/DTA results of LCM55 and LSCM6512 respectively. The TGA curves show about 60% mass loss within first 250 °C. The second and third mass loss regions of 5% and 2% in the temperature range of 550–650 °C and 650–750 °C, respectively are also visible. In the DTA curve, an exothermic peak is found at 285 °C for LCM55 whereas a similar kind of peak is observed at 280 °C for LSCM6512 sample..

3.2. X-ray diffraction

XRD patterns of the $La_{(1-x)}Ca_xMnO_3$ (x = 0.3 to 0.5) and $La_{0.65}Sr_yCa_{(0.3-y)}MnO_3$ (y = 0.1 to 0.2) powder samples calcined at 800 °C for 12 h are shown in Fig. 2a. XRD patterns indicate that a single phase is formed for all compositions. All compositions can be indexed as orthorhombic symmetry. Extra peaks are not observed in the figures. However, it can be noted that with the increase of Ca-content the peaks shift to a higher 2Θ value [Fig. 2a. (a)–(c)] for LCM samples though for LSCM [Fig. 2a. (d)–(f)] samples peak shifting is not discernable..

Further the interaction between LCM55 and YSZ was studied at SOEC operating condition and cell fabrication temperature. A thoroughly ball milled 1:1 mixture of LCM and YSZ was heat treated at 1000 °C for 100 h. Fig. 2b shows XRD pattern after heating the power mixture. Other than the characteristics peaks of YSZ and LCM no other peaks are visible in the figure.

3.3. Shrinkage behavior

To identify the proper sintering temperature of the samples, shrinkage behavior of one composition (LCM55) was studied by dilatometer from room temperature to 1350 °C. Fig. 3 indicates that there is no shrinkage up to 850 °C and above this temperature shrinkage occurs and it increases up to 1300 °C. No further shrinkage is observed after that temperature..

3.4. Sintering

Theoretical densities as measured by He-Pycnometry and relative densities as measured by Archimedes principle after sintering the samples at 1300 °C for 3 h are given in Table 1. The theoretical densities of all the samples are in the range from 6.0 to 6.3 g/cm^3. The relative densities of all the samples are in the range from 89% to 98% of the theoretical density. For both group of materials, relative densities increase with the increase in Ca-concentration.

3.5. Thermal expansion coefficient (TEC)

Fig. 4 shows the thermal expansion behaviors of all the composition. The thermal expansion curves are almost linear in the temperature range from 450 °C to 950 °C. The average TECs of all the samples in the temperature range from 100 °C to 900 °C are given in Table 1. TEC values are in the range of 11–12×10^{-6} K^{-1}..

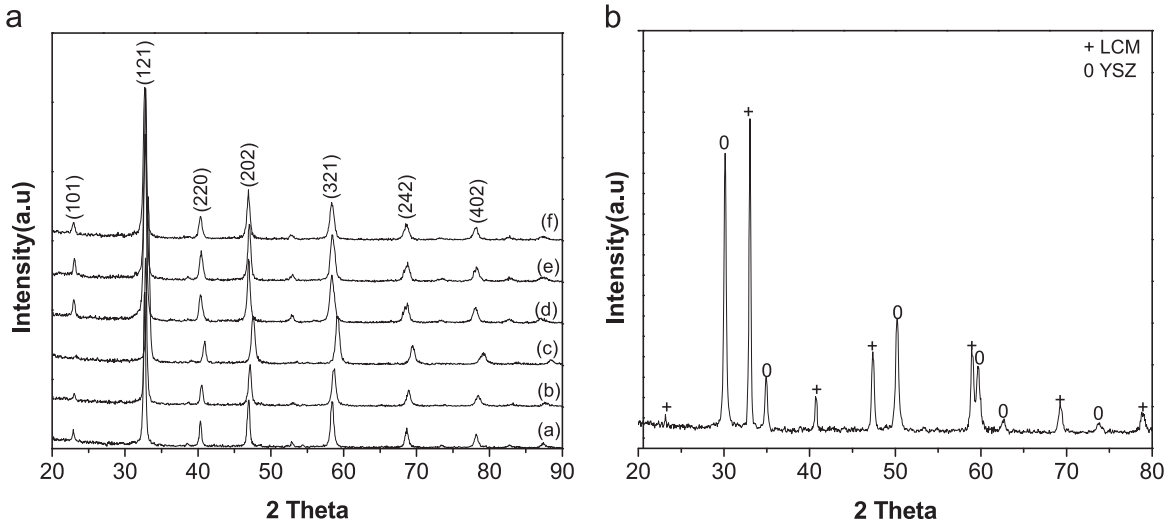

Fig. 2. a: XRD patterns of (a) LCM73, (b) LCM64, (c) LCM55, (d) LSCM6521, (e) LSCM651515, (f) LSCM6512. b: XRD patterns of LCM and YSZ powders heat treated at 1000 °C for 100 h.

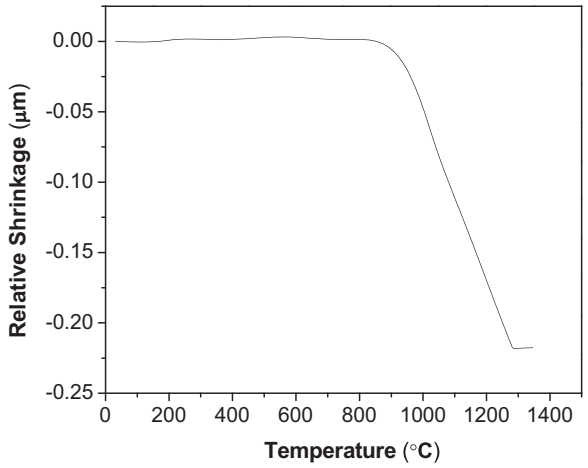

Fig. 3. Shrinkage behavior of LCM55 as a function of temperature.

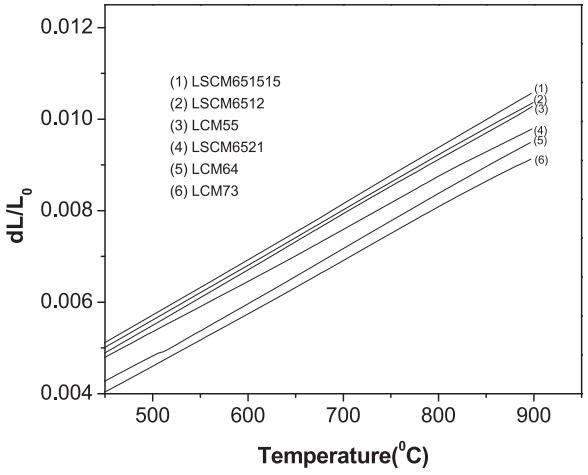

Fig. 4. Thermal expansion behavior as a function of temperature.

3.6. Electrical conductivity

Fig. 5 shows the measured electrical conductivities of the as sintered samples with different Sr and Ca content as a function of reciprocal of temperature. The conductivities increase with temperature, as expected in a semiconducting material. The Arrhenius plot of ln(σT) vs 1/T of all samples exhibits a linear dependence over the temperature range from 750 °C to 950 °C (operating temperature of

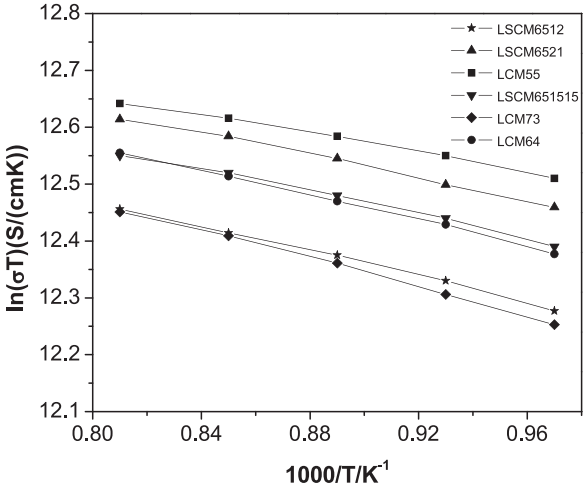

Fig. 5. Electrical conductivity as a function of reciprocal temperature.

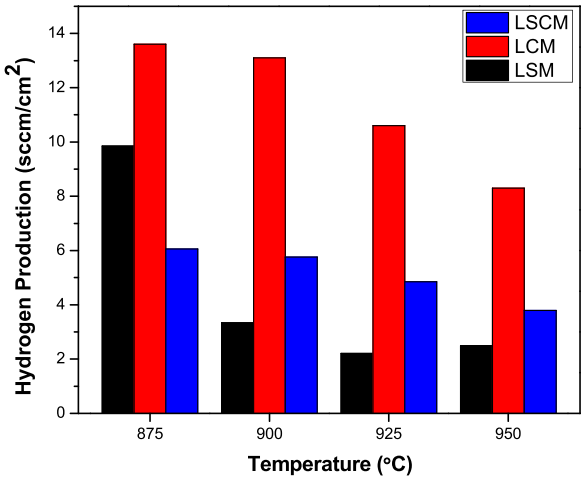

Fig. 6. Hydrogen production of LSM, LCM55 and LSCM6512 anodes after being tested in a SOEC set up. Hydrogen production of LSM anode is taken from Ref [19].

electrolysis), as predicted by the equation:

$$\ln(\sigma T) = \ln A - \frac{E_a}{RT}$$

where σ, A, T, R and E_a are the conductivity of the material, pre-exponential factor, absolute temperature, gas constant and activation enthalpy for the conduction. It is also clear from Fig. 5 that conductivity increases with increasing Ca-content for LCM samples but for LSCM samples conductivity decreases with increasing Ca-content. The highest conductivity obtained for LCM55 sample is ~265 S/cm at 950 °C. The conductivity values for different samples at 950 °C are reported in Table 1..

3.7. Electrolysis performance

To check the electrolysis performance, newly synthesized materials were used as anode materials in coupon cells. The electrolysis performances of the newly synthesized materials are compared with LSM. Fig. 6 shows the production of hydrogen of LSM, LCM55 and LSCM6512 respectively. Comparing the hydrogen production (Fig. 6), it can be noticed that the amount of produced hydrogen is more for LCM samples than LSCM sample. Moreover, unlike LSM anode the loss of hydrogen production with increase in temperature is comparatively gradual..

4. Discussion

Ca doped $LaMnO_3$ was synthesized using combustion synthesis method. This method was employed to get ceramic powders at lower calcination temperature and at relatively shorter time. The formation of the gel is a prerequisite for the intimate blending of the starting constituents. After the gel formation it was collected and studied using TGA and TDA [Fig. 1a and b]. The TGA profile represents the decomposition stages. The first stage from 50 °C to 250 °C is due to the loss of water and volatile organic species. The second stage, from 550 °C to 650 °C, is due to the decomposition of carbonates species [21,22]. In the DTA curves the exothermic peak at 280 °C and 285 °C are due to the loss of water and volatile organic species which is also supported by the mass loss in the TGA curve. Also, as there is no weight loss after 750 °C, it is expected that calcination temperature above 750 °C will be necessary for single phase formation. In the present work, calcination temperature of the powders was chosen at 800 °C with the expectation of the single phase material formation. To check the phase formation XRD diffraction studies were carried out for the as calcined samples [Fig. 2a]. The samples are identified to have orthorhombic structure. As the Goldschmidt tolerance factor of the

Ca-doped lanthanum manganite perovskite is lower than unity [23,24], as Ca^{2+}(134 pm) is smaller than La^{3+}(136 pm) [25], it is expected that samples will show lower symmetry other than cubic. Consequently, it is not surprising that our samples also show orthorhombic symmetry. Moreover, it is obvious that substitution of La^{3+} by smaller Ca^{2+} will decrease the lattice volume which in turn will increase the diffraction angle. Consequently, as the Ca content increases from LCM 73 to LCM 55 the peak shifts to a higher 2θ value [Fig. 2a].

Coming to sintering, the shrinkage behavior curve (Fig. 3) suggests that a minimum of 1300 °C is needed for the sintering of the samples. Accordingly all the samples of the present work were sintered at 1300 °C for 3 h. Contrasting role of Ca and Sr towards sintering behavior matches well with the surface area of the samples (Table 1). It is clear that with the increase of Ca-content surface area increases for LCM samples [Table 1]. But in the case of LSCM samples increase in surface area is insignificant with the increase in Ca-content. It means higher is the surface area higher is the driving force for sintering and higher is the relative density as can be evinced from Table 1. Moreover, the diffusion rate in the solid state is related to the ionic radius of the cation. Rooselman et al. [26] reported that small ions will diffuse faster and will tend to shift the sinter curves to lower temperatures. Concomitantly, the density of the smaller ion containing species will be high. Our results also suggest that the relative density is higher for Ca-containing species compared to the Sr-containing species.

As a SOEC is an assembly of a cathode, anode and electrolyte it is imperative that all the constituents need to have matching TEC to avoid any thermal stress. So, the TEC of the as sintered samples were measured [Fig. 4]. It is noticed that TEC values increase with the increase in Ca content irrespective of partial or total substitution of Sr by Ca. As La^{3+} is replaced by smaller size Ca^{2+}, O^{2-} vacancy in the lattice is created. Electrostatic attraction and repulsion forces within the lattice determine the thermal expansion of the material. These forces are the function of the positive and negative charges and their locations in the lattice [14]. So, the thermal expansion increases if the attraction forces decrease. Now, for a definite crystal structure and at a fixed oxygen/metal stoichiometric composition, the TEC is characterized only by the lattice vibrations. However, if there is loss of oxygen due to an increase in temperature or due to a reducing atmosphere then thermal expansion will be increased as has been shown in Fig. 4. Loss of oxygen increases the ionic mobility of the cations, which in turns increases the TEC. So, more is the amount of Ca, more is the amount of O^{2-} vacancy with the concomitant effect of more is the TEC. The TEC values of the present material are almost close to the TEC value of 8YSZ electrolyte ($9–11\times10^{-6}\ K^{-1}$) and Ni-YSZ ($10.5–14\times10^{-6}\ K^{-1}$) [4] making them suitable as anode materials.

Electrical conductivity, another important property of an anode material of a SOEC, is given in Fig. 5. The linearity of the plot (Fig. 5) indicates that the conductivity mechanism is by thermally activated hopping of small polarons [20]. Increase of conductivity with the increase in Ca content for LCM samples but the decrease of it by increasing the same in LSCM samples can be explained in the following way. $LaMnO_3$ is an intrinsic p-type semiconductor. Substitution of La^{3+} by lower valance cation such as Sr^{2+} or Ca^{2+} increases the oxidation number of Mn^{3+} ion. Mn ions can remain in Mn^{2+}, Mn^{3+} and Mn^{4+} states [27]. Normally it tends to remain as Mn^{3+} in atmospheric condition. When La^{3+} is substituted by Ca^{2+} or Sr^{2+} ions then to maintain the electro-neutrality condition there occurs either an increase in oxidation number of Mn^{3+} ion in B-site or the generation of an electron hole in the B-site. The possible equations are given as follows

$$LaMnO_3 \xrightarrow{xCaO} La^{3+}_{1-x}Ca^{2+}_{x}Mn^{3+}_{1-x}Mn^{4+}_{x}O_3$$

$$2CaO+Mn_2O_3+½O_2\ (g) \xrightarrow{LaMnO_3} 2\ Ca'_{La}+2Mn^{x}_{Mn}+6O^{x}_{O}+2h^{\bullet}$$

When this types of substitution happens, Mn^{3+} combines with an electron hole to form Mn^{4+} ion ($Mn^{3+}+h^{\bullet} \rightarrow Mn^{4+}$) resulting an increase in electronic conductivity of (La, Ca)MnO_3. Moreover, charge neutrality may be through oxygen vacancy. The possible equation is

$$2CaO+Mn_2O_3 \xrightarrow{LaMnO_3} 2\ Ca'_{La}+2Mn^{x}_{Mn}+5O^{x}_{O}+V^{\bullet\bullet}_{O}$$

When two Mn^{4+} ions get reduced to Mn^{3+} ion an oxygen vacancy is created and O^{2-} conduction occurs. With the increase of Ca-content at the La-site more electron hole and oxygen vacancy created which consequently increases the conductivity, as has been shown in Fig. 5. Activation enthalpy values (Table 1) also support this. Wu et al. [28] reported that both the oxidation of Mn^{3+} to Mn^{4+} and formation of oxygen vacancy take place in $La_{(1-x)}Ca_xMnO_3$ (LCM) system for NH_3 oxidation. Therefore, it is believed that both the charged hole and oxygen vacancy may make the contribution to the electrical conductivity of LCM in the present investigation. Moreover, as far as conductivity is concerned full substitution of Sr by Ca is better than partial substitution. Also, due to its reasonably high electrical conductivity it can be used as an anode material in SOEC.

It goes without saying that chemical compatibility between an electrolyte and electrode materials is a must for the successful operation of a SOEC. Accordingly, chemical compatibility between YSZ and LCM was checked [Fig. 2b]. It is found that YSZ and LCM do not react even after heating at 1000 °C for 100 h. It may be concluded that YSZ and LCM are chemically compatible at least up to 100 h.

The size mismatch between the dopant and host cations plays an important role in terms of elastic energy minimization. In fact, elastic and electrostatic interactions of the dopant with the surrounding lattice of the perovskite material are responsible for the surface segregation, which consequently makes the doping phenomenon feasible by lowering the free energy of the system [29]. Further, Lee et al. [29] demonstrated that the size mismatch between the dopant host cations contribute significantly to the segregation of the dopant cations and concomitant secondary phase formation at the surface. Naturally, Ca^{2+} in place of Sr^{2+} will minimize the elastic energy because the Sr^{2+} differs highly from the La^{3+}, whereas the size of the Ca^{2+} does not differ much from the La^{3+}. It is obvious that by varying only the size of the dopant cation the elastic energy differences in the system was systematically induced without disturbing the electrostatic interactions of the dopant as Sr^{2+} and Ca^{2+} have same charge. It means chances of surface segregation are less with Ca^{2+} containing samples than its Sr^{2+} containing counterpart. In line with the above mentioned discussion, we find that LCM does react with YSZ but LSM is reported to do so [19]. However, further long term tests need to be carried out for drawing out any far reaching conclusion. Based on the foregoing discussion, it can be proposed that LCM may be a very promising material to be used as an anode for SOEC.

In our earlier study [19], we have reported the poor performance of LSM anode in a SOEC due to the formation of non-conducting secondary phases like lanthanum zirconate and yttrium silicate at the anode and cathode side respectively. However, comparing the hydrogen production (Fig. 6), it can be noticed that the amount of produced hydrogen is more for LCM samples than LSCM sample. Moreover, unlike LSM anode the loss of hydrogen production with increase in temperature is comparatively gradual, indicating the higher sustainability of the material as an anode of SOEC. Thus, anode materials with either partial or total substitution of Sr by Ca seem to be better than LSM. Also, based on the above results it may be concluded that among the Ca containing materials total substitution of Sr by Ca may be even better choice as anode material.

5. Conclusion

In search of a new anode material for SOEC, a series of materials, where Sr of LSM was either partially or fully substituted by Ca, were

synthesized via combustion synthesis method. The synthesized material was found to be phase pure with orthorhombic symmetry. Thermal expansion coefficients (TEC) of all the samples were found to be in the range of $11–12\times10^{-6}\,K^{-1}$ which is very close to routinely used electrolyte YSZ. Ca-doped $LaMnO_3$ seems to be chemically compatible with YSZ electrolyte as no reaction product was found by XRD even after a prolong annealing of 100 h at 1000 °C. This is attributed to minimization of elastic energy as Sr^{2+} differs highly from the La^{3+}, whereas the size of the Ca^{2+} does not differ much from the La^{3+}. Samples show adequate electrical conductivity necessary for an anode material. Also, electrical conductivity was found to increase with increasing Ca-content for the samples where Sr was fully replaced by Ca (LCM) but the same was found to decrease with increasing Ca-content for the partially Sr substituted samples (LSCM). However, comparing the hydrogen production from the SOEC using the newly synthesized materials as anode shows produced hydrogen is more for LCM sample than LSCM sample. Present investigation suggests that Ca doped $LaMnO_3$ material may be a promising anode material for SOEC.

Acknowledgements

The authors would like to thank Director, CSIR-Central Glass and Ceramic Research Institute for giving his consent to publish this work. One of the authors, AM also acknowledges the technical support rendered to him by the Staff members of Fuel Cell and Battery Division.

References

[1] J.E. O'Brein, C.M. Stoots, J.S. Herring, J.J. Hartvigsen, Hydrogen production performance of a 10-cell planar solid-oxide electrolysis stack, J. Fuel Cell Sci. Technol. 3 (2006) 213–219.
[2] A. Hauch, S.H. Jensen, S. Ramousse, M. Mogensen, Performance and durability of solid oxide electrolysis cells, J. Electrochem. Soc. 153 (2006) A1741–A1747.
[3] R. Rivera-Tinoco, C. Mansilla, C. Bouallou, Competitiveness of hydrogen production by High Temperature Electrolysis: impact of the heat source and identification of key parameters to achieve low production costs, Energy Convers. Manag. 51 (2010) 2623–2634.
[4] N.Q. Minh, Ceramic fuel cells, J. Am. Ceram. Soc. 76 (1993) 563–588.
[5] P. Singh, N.Q. Minh, Solid oxide fuel cells: technology status, Int. J. Appl Ceram. Technol. 1 (2004) 5–15.
[6] A.J. Jacobson, Materials for solid oxide fuel cells, Chem. Mater. 22 (2010) 660–674.
[7] M.C. Williams, Solid oxide fuel cells: fundamentals to systems, Fuel Cells 7 (2007) 78–85.
[8] S.P. Jiang, J.P. Zhang, K. Foger, Chemical interactions between 3 mol% yttria-zirconia and Sr-doped lanthanum manganite, J. Eur. Ceram. Soc. 23 (2003) 1865–1873.
[9] A. Chen, G. Bourne, K. Sieben, R. DeHoff, E. Wachsman, K. Jones, Characterization of lanthanum zirconate formation at the A-site-deficient strontium-doped lanthanum manganite cathode/yttrium-stabilized zirconia electrolyte interface of solid oxide fuel cells, J. Am. Ceram. Soc. 91 (2008) 2670–2675.
[10] M. Keane, M.K. Mahapatra, A. Verma, P. Singh, LSM–YSZ interactions and anode delamination in solid oxide electrolysis cells, Int. J. Hydrog. Energy 37 (2012) 16776–16785.
[11] S. Carter, A. Selcuk, R.J. Chater, J. Kajda, J.A. Kilner, B.C.H. Steele, Oxygen transport in selected nonstoichiometric perovskite-structure oxides, Solid State Ion. 53–56 (1992) 597–605.
[12] R.A. De Souza, J.A. Kilner, J.F. Walker, A SIMS study of oxygen tracer diffusion and surface exchange in $La_{0.8}Sr_{0.2}MnO_{3+\delta}$, Mater. Lett. 43 (2000) 43–52.
[13] V.V. Srdic, R.P. Omorjan, J. Seydel, Electrochemical performances of $(La,Sr)CoO_3$ cathode for zirconia-based solid oxide fuel cells, Mater. Sci. Eng. B 116 (2005) 119–124.
[14] H. Ullmann, N. Trofimenko, F. Tietz, D. Strover, A. Ahmad-Khanlou, Correlation between thermal expansion and oxide ion transport in mixed conducting perovskite-type oxides for SOFC cathodes, Solid State Ion. 138 (2000) 79–90.
[15] Y. Takeda, Y. Sakaki, T. Ichikawa, N. Imanishi, O. Yamamoto, Stability of $La_{1-x}AxMnO_{3-z}$ (A=Ca, Sr) as cathode materials for solid oxide fuel cells, Solid State Ion. 72 (1994) 257–264.
[16] Z. Jie, L.I. Chen, K. Linglong, W.U. Xuewei, M.A. Yongchang, Synthesis and characterization of calcium and manganese-doped rare earth oxide $La_{1-x}CaxFe_{0.9}Mn_{0.1}O_{3-\delta}$ for cathode material in IT-SOFC, J. Rare Earths 29 (2011) 1066–1069.
[17] H. Yokokawa, N. Sakai, T. Horita, K. Yamaji, Recent developments in solid oxide fuel cell materials, Fuel Cells 1 (2001) 117–132.
[18] R.N. Basu, A.D. Sharma, A. Dutta, J. Mukhopadhyay, Processing of high performance anode-supported planar solid oxide fuel cell, Int. J. Hydrog. Energy 33 (2008) 5748–5754.
[19] A. Mahata, P. Datta, R.N. Basu, Microstructural and chemical changes after high temperature electrolysis in solid oxide electrolysis cell, J. Alloy Compd. 627 (2015) 244–250.
[20] A. Kumar, P.S. Devi, H.S. Maiti, Effect of metal ion concentration on synthesis and properties of $La_{0.84}Sr_{0.16}MnO_3$ cathode material, J. Power Sources 161 (2006) 79–86.
[21] A. Ghosh, A.K. Sahu, A.K. Gulnar, A.K. Suri, Synthesis and characterization of lanthanum strontium manganite, Scr. Mater. 52 (2005) 1305–1309.
[22] Z. Gaoke, L. Ying, Y. Xia, W. Yanping, S. Ouyang, L. Hangxing, Comparison of synthesis methods, crystal structure and characterization of strontium cobaltite powders, Mater. Chem. Phys. 99 (2006) 88–95.
[23] L. Malavasia, M.C. Mozzatib, C.B. Azzonib, G. Chiodellia, G. Flora, Role of oxygen content on the transport and magnetic properties of $La_{1-x}Ca_xMnO_{3+d}$ manganites, Solid State Commun. 123 (2002) 321–326.
[24] L. Malavasi, Role of defect chemistry in the properties of perovskite manganites, J. Mater. Chem. 18 (2008) 3295–3308.
[25] R.D. Shannon, Revised effective ionic radii and systematic studies of interatomic distances in halides and chalcogenides, Acta Crystallogr. A 32 (1976) 751–767.
[26] J.A.M. van Roosmalen, E.H.P. Cordfunke, J.P.P. Huijsmans, Sinter behaviour of (La, Sr)MnO_3, Solid State Ion. 66 (1993) 285–293.
[27] S. Fritsch, A. Navrotsky, Thermodynamic properties of manganese oxides, J. Am. Ceram. Soc. 79 (1996) 1761–1768.
[28] Y. Wu, T. Yu, B.S. Dou, C.X. Wang, X.F. Xie, Z.L. Yu, S.R. Fan, Z.R. Fan, L.C. Wang, A comparative study on perovskite-type mixed oxide catalysts $A'xA_{1-x}BO_{3-\lambda}$ (A′=Ca, Sr, A=La, B=Mn, Fe, Co) for NH_3 oxidation, J. Catal. 120 (1989) 88–107.
[29] W. Lee, J. Woo Han, Y. Chen, Z. Cai, B. Yildiz, Cation size mismatch and charge interactions drive dopant segregation at the surfaces of manganite perovskites, J. Am. Chem. Soc. 135 (2013) 7909–7925.